

# Thermal-mechanical behaviour during initial solidification in continuous casting: steel grade effects

J. Sengupta<sup>1</sup>, C. Ojeda<sup>2</sup> and B. G. Thomas\*<sup>3</sup>

A transient finite-element model (CON2D) is applied to compute temperature, stress, and distortion of the steel shell during initial solidification. The model incorporates temperature-dependent properties, thermal shrinkage, phase transformations, and different elastic-viscoplastic constitutive equations for each phase (liquid,  $\delta$ , and  $\gamma$ ). The effects of sudden metal level fluctuations are simulated for different steel grades. Increasing the depth of a level drop increases distortion of the shell tip, curving it further away from the mould wall. This curvature is largest for ultra-low-carbon (ULC) and peritectic steels, and decreases for low- and high-carbon steels. This matches the well-known plant observations of the variation of oscillation mark depth with steel grade. The results suggest that the shape of the lower side of oscillation marks is governed by thermal distortion, which is greatly aggravated by level fluctuations.

**Keywords:** Continuous casting, Meniscus, Oscillation marks, Hooks, Steel grade, Peritectic

## Introduction

Initial solidification at the meniscus is of great importance to the quality of continuous-cast steel because it forms the surface of the final product. The common surface features, oscillation marks and subsurface hooks, are pictured in Fig. 1,<sup>1</sup> and are often associated with quality problems such as inclusion entrapment and cracks. They are controlled by the changes in heat transfer, fluid flow, pressure, and thermal stresses that occur near the meniscus during each mould oscillation cycle. These phenomena are sketched in Fig. 2.

Many previous efforts have been made to understand initial solidification of steel, including work by many top researchers of continuous casting: Kurz,<sup>2</sup> Brimacombe,<sup>3,4</sup> Samarasekera,<sup>5</sup> Wolf,<sup>6</sup> Lesoult,<sup>7</sup> Cramb,<sup>8</sup> Schwerdtfeger,<sup>9</sup> Fredriksson,<sup>10</sup> and others,<sup>11–13</sup> which has been recently reviewed.<sup>2,7</sup> Oscillation mark formation with curved hooks has been shown to involve meniscus freezing, followed by liquid steel overflow into the gap.<sup>8,12</sup> Sometimes, the overflowing steel may solidify and stick to the mould wall, to be stripped off and welded to the lower shell during the negative strip time.<sup>14</sup> The known importance of negative strip suggests that the latter mechanism must occur at least in a few percent of the cycles, and seems even more likely with oil lubrication. Mechanical bending of the initially solidified shell has also been proposed. However, significant

bending seems unlikely, because steel near the solidus temperature is very brittle. Moreover, this mechanism is inconsistent with the 3-D shape of hooks observed in the corner, which accompany oscillation marks that point down (in the casting direction) and are due to deeper overflow of a 3-D curved frozen meniscus.<sup>15</sup> Pressure variations in the flux channel, and the solid slag rim shape are known to affect oscillation mark depth,<sup>3,4</sup> likely by altering the liquid meniscus shape. Thermal distortion has been shown to be capable of generate deep transverse depressions.<sup>11</sup> Its affect on oscillation mark formation has not been studied.

Steel composition is well-known to affect surface shape, owing to the shrinkage of the peritectic phase transformation. Ultra-low-carbon (ULC) steels (%C<0.01%) and peritectic steels (0.09–0.17%C) have the deepest oscillation marks,<sup>8</sup> while low and high carbon steels have much flatter surfaces. Hooks increase in depth with decreasing carbon content below 0.15%C.<sup>3,4</sup> However, the details of why these grade effects occur, and the mechanisms of how oscillation marks and hooks form are not fully understood. Thus, this work simulates thermal distortion of the solidifying shell due to fluctuations in mould level, and investigates the effect of steel grade.

## Model description

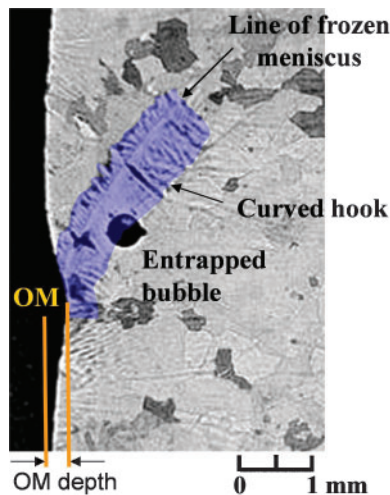
Thermal and mechanical behaviour of a longitudinal slice through the solidifying steel shell is simulated as it moves down the mould wall at the casting speed using the transient, thermal-elastic-viscoplastic finite-element model, CON2D.<sup>16</sup> It is applied here to simulate thermal distortion near the meniscus, including the effects of a fluctuation in the liquid level.

<sup>1</sup>Global R&D Hamilton, ArcelorMittal Dofasco, Hamilton, Ontario, Canada

<sup>2</sup>Centre for Research in Metallurgy (CRM), Liege, Belgium

<sup>3</sup>Department of Mechanical Science and Engineering, University of Illinois, 1206 West Green St., Urbana, Illinois, USA

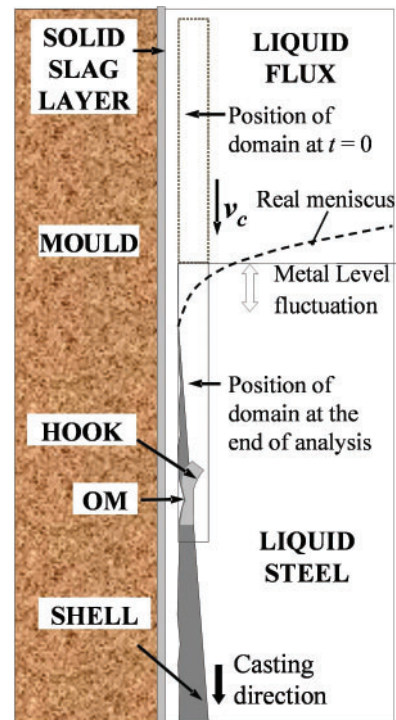
\*Corresponding author, email bgthomas@uiuc.edu



1 Typical oscillation mark and hook in section through solidified slab (ULC steel)

The model solves the two-dimensional (2-D) transient energy equation using a fixed Lagrangian grid of 3-node triangular elements, incorporating latent heat through spatial averaging of the enthalpy and temperature gradients. The mechanical equilibrium equations are solved after interpolating the thermal loads onto a mesh of 6-node triangles. The out-of-plane ( $y$ ) perimeter-direction stress is characterized by the state of generalized plane strain, which reasonably approximates the complete 3-D stress state, for the wide, thin shell of interest. Nucleation under-cooling is ignored, so meniscus solidification is not considered.

Constitutive equations for plain-carbon steel include the rate-dependent, elastic-viscoplastic model III of Kozłowski<sup>17</sup> for austenite and the modified power law of Zhu for delta-ferrite.<sup>11</sup> These equations vary with temperature and carbon content, and were fit to match several sets of experimental data. They are integrated using a special two-level algorithm, which alternates between solutions at the local node point and the global system equations.<sup>16</sup> Liquid elements, defined by the specified coherency temperature, are set to have no elastic strain, and inelastic strain is reset to zero at the solidus temperature. Temperature-dependent functions for enthalpy, thermal conductivity, elastic modulus, and thermal linear expansion are provided elsewhere.<sup>16</sup> Thermal conductivity is increased linearly through the



2 Meniscus region showing downward movement of rectangular finite-element domain

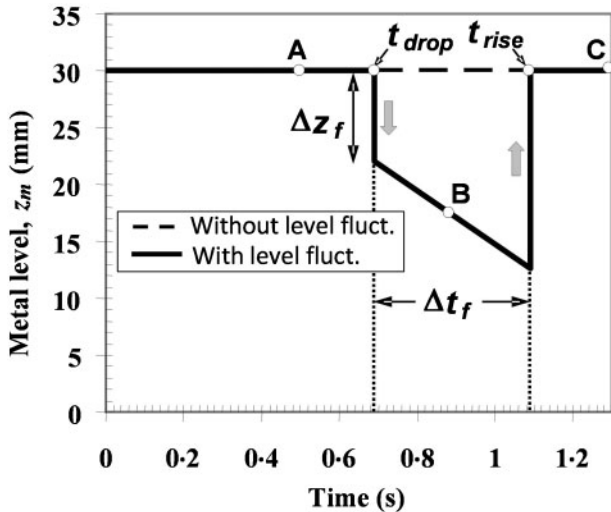
mushy zone to 6.5 times its nominal value in the liquid to roughly approximate the effects of convection. Phase fractions of liquid, ferrite, and austenite evolve according to a simple microsegregation model.<sup>18</sup> Corresponding liquidus and solidus temperatures for each grade are given in Table 1. Further details and validation of this model using both analytical solutions and measurements from operating casters is described elsewhere.<sup>16</sup>

The  $3 \times 30$  mm model domain, shown in Fig. 2, initially contains stress-free liquid at uniform temperature. The shell solidifies continuously below an idealized sharp, flat meniscus and moves downward at the casting speed. Thus, below the meniscus on the mould side, heat flux to the mould at  $T_m$  is defined by a simple convection coefficient,  $h_m$ , while all other domain boundaries have zero heat flux.

The time variation of the liquid metal level is shown in Fig. 3. As the domain moves downward, the metal level

Table 1 Simulation conditions

Steel Grades	Liquidus (°C)	Solidus (°C)	Range (°C)
Ultra-low carbon steel (0.003%C, 0.08Mn, 0.009S)	1533.9	1519.3	14.6
Low carbon steel (0.04%C, 0.2Mn, 0.02Si, 0.018S)	1529.3	1520.4	33.6
Peritectic steel (0.13%C, 0.5Mn, 0.015Si, 0.015S)	1495.7	1464.9	55.5
Casting conditions:			
Superheat temperature difference	30°C		
Casting speed	23.33 mm s <sup>-1</sup> (1.42 m min <sup>-1</sup> )		
Mould oscillation	Frequency: 2.58 Hz (155 cpm)		
	Stroke: 6.34 mm		
Negative strip time	~0.4 s		
Mould temperature, $T_m$	250°C		
Mould / shell heat transfer coefficient, $h_m$	4000 W m <sup>-2</sup> K <sup>-1</sup>		
Level fluctuation duration ( $\Delta t_f$ )	0.4 s		
Height of level drop/rise ( $\Delta z_f$ )	2–16 mm		
Liquid flux temperature (during fluctuation), $T_f$	1000°C		
Liquid flux / shell heat transfer coefficient (during fluctuation), $h_f$	1500 W m <sup>-2</sup> K <sup>-1</sup>		



**3 Metal surface level history during a simulated level fluctuation in lab (stationary) frame of reference. Instants A, B, and C occur before, during, and after level drop**

in the shell frame of reference during steady casting is simply the casting speed multiplied by time. After the shell has moved downward 16 mm (0.69 s), the liquid level is suddenly dropped for 0.4 s. This roughly approximates the duration of small level fluctuations that might occur during each oscillation cycle or it could also represent a random flow transient. During this time ( $t_{drop} < t < t_{rise}$ ) the inner edge of the solidifying shell is exposed to the molten slag layer that floats above the liquid steel. Liquid elements are ignored and heat flux from the exposed solid shell to the slag at  $T_f$  is defined by convection coefficient,  $h_f$ . At  $t_{rise} = 1.09$  s, the level is raised up to the shell tip (now at  $z = 25$  mm) by restoring the liquid elements at the initial temperature, and allowing solidification to continue. Overflow of the meniscus is not simulated. Conditions are given in Table 1.

No surface forces or constraints were applied, except for fixing three nodal displacement degrees-of-freedom at the domain bottom to prevent rigid body motion. This stress-free condition assumes that pressure in the flux channel roughly balances ferrostatic pressure (both  $\sim 1\text{--}2$  kPa), and neglects the effects of their variations. A mesh of  $31 \times 61$  nodes with  $0.1 \times 0.5$  mm elements was used, after a mesh refinement study with finer meshes and larger domains revealed no major differences in the results.

## Results

Fig. 4 shows temperature contours and shell tip shape at three representative times during a typical level fluctuation for ULC steel: (A) 0.19 s before the level drops, (B) 0.21 s after the level drops, and (C) 0.21 s after the level rises again (meniscus overflow). Corresponding temperature and stress profiles through this shell are shown in Fig. 5 at 5 mm above the domain bottom. Stresses are all very low, less than 1 MPa, due to the rapid creep relaxation in soft delta-ferrite at these high temperatures, and the lack of mechanical constraint. Interior stresses near the solidification front are even lower, so can be lost in the numerical noise of the simulation.

Thus, these results reveal the more important effect on the shape of the solidifying shell near the tip.

### During solidification

During steady casting, the surface initially cools rapidly, which causes slight tension at the surface. This distorts the shell tip towards the mould wall. As the shell tip should always touch the wall, the resulting shape is concave towards the mould, with a  $\sim 0.02$  mm-deep depression. This thin gap could significantly lower local heat transfer, although this effect was not modelled here.

These results contrast with behavior later during solidification, (further below the shell tip), when the surface cooling rate slows. In this case, reported elsewhere,<sup>19,20</sup> the surface temperature drops slowly relative to the interior. Then, subsurface cooling and contraction generates subsurface tension, which induces compression at the shell surface. This tends to reverse shell distortion, presenting a slightly convex shape toward the mould walls.

### During drop in level

After the level drops suddenly at 0.69 s by  $\sim 16$  mm, the liquid-steel side of the shell is exposed to mould flux. Without the heat supplied from the molten steel, the mould extracts sensible heat from the thin shell very quickly. Temperature throughout the shell tip drops rapidly ( $\sim 200$  °C in 0.19 s). Thermal gradients inside the shell disappear, as temperature within the thin shell equilibrates. This means that the shell interior cools and contracts more than the outside, causing the shell tip to bend away from the mould. This leaves a convex shape facing the mould wall.

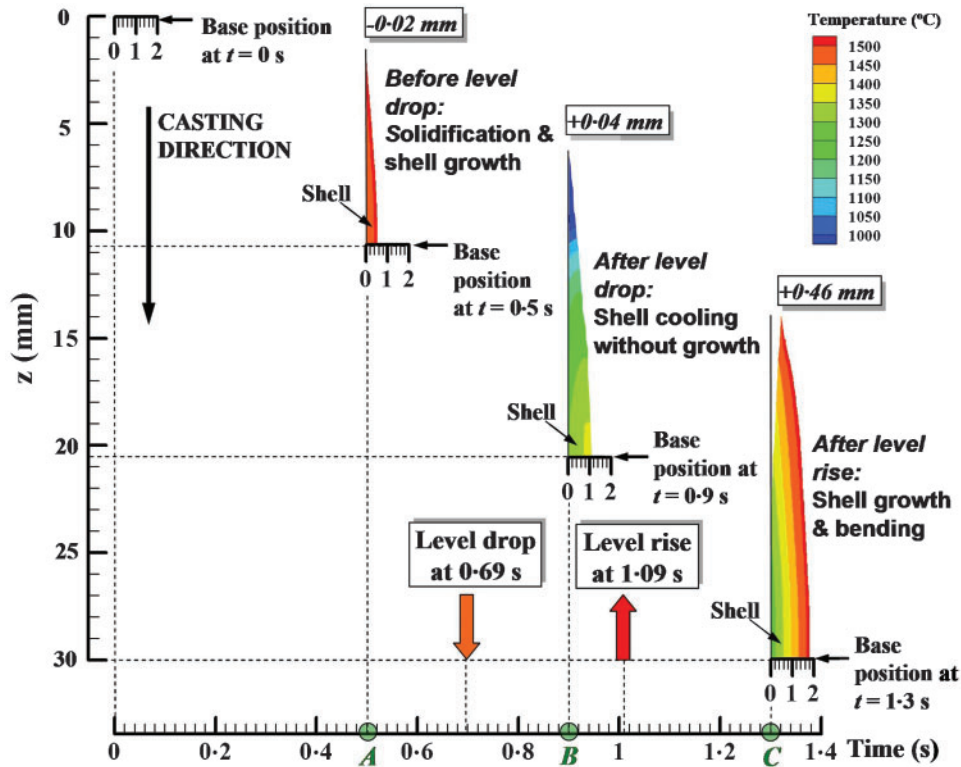
### After rise in level

Raising the liquid level back up to the shell tip causes a rapid increase in temperature, shell thickness, and distortion (Figs. 4c and 5c). Liquid steel contacts and solidifies a new skin over the older cold shell tip. The older shell expands due to its substantial reheating, but may be constrained by the new skin, which is cooling and contracting. If this new layer is strong enough, the shell tip distorts substantially towards the liquid steel, like a bimetallic strip. In this ULC steel example, tip deflection reaches 0.46 mm in just 0.21 s. This large tip deflection indicates that thermal distortion from level fluctuations is an important mechanism for changing the shape of the shell tip.

These findings suggest that a similar shell distortion would occur if a precariously balanced liquid steel meniscus overflows the shell tip or frozen meniscus during oscillation mark formation. This would increase the curvature of the frozen meniscus.

### Level fluctuation severity effects

The example level drop of 16 mm chosen to demonstrate thermo-mechanical behavior during a level fluctuation, occurs only rarely in a good commercial casting operation. Most level fluctuations are less than 10 mm. Figure 6 shows the effect of varying the depth of the level drop, keeping the duration constant at 0.4 s. Deeper or longer level fluctuations produce more bending due to this thermal distortion effect. The extreme case of the level drop during tail-out at the end of a casting sequence produces several centimetres



4 Evolution of temperature and shell tip distortion during a level fluctuation event

of tip distortion. For small level fluctuations, the shell tip deflection is almost negligible.

Another effect of a level fluctuation is to produce a slight jog in the shape of the shell thickness profile, at the junction between the top region (that was exposed to mould slag), and the lower region (that solidifies normally). If the liquid level never rises completely back to the top of the old shell, then the jog is more extreme. A similar-shaped jog was observed near the tip of a breakout shell (Fig. 7).

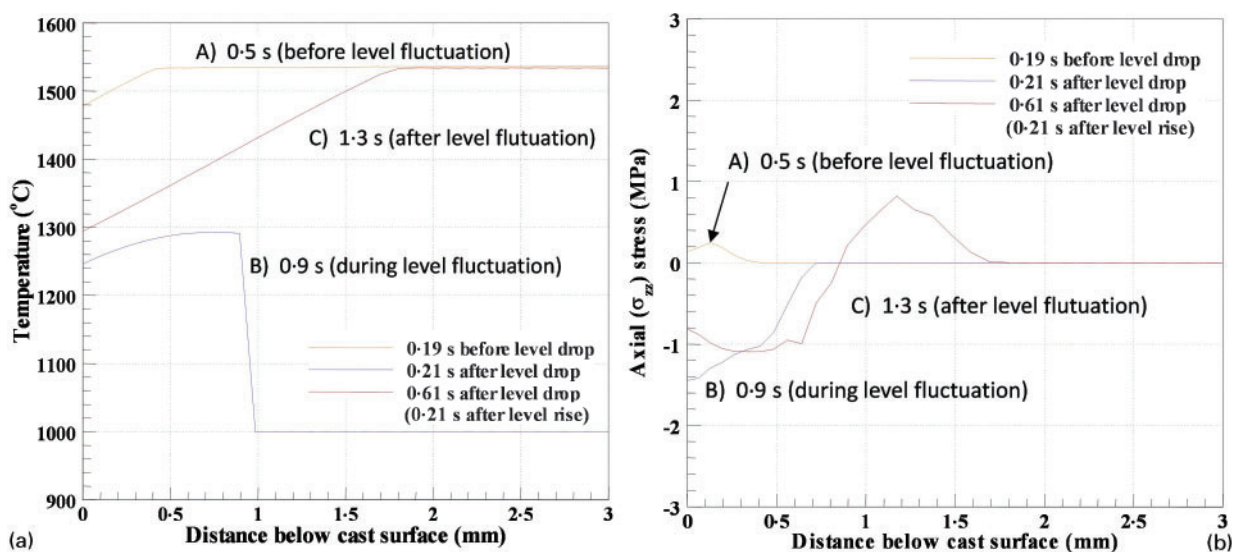
### Steel Grade Effects

Figure 8 shows the effect of steel grade on temperature and distorted shape, both before and after a level

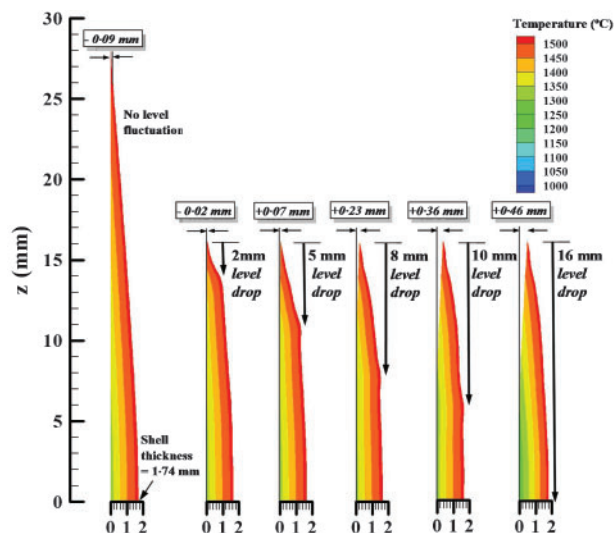
fluctuation of 16 mm for 0.4 s. In addition to the ULC case study, results for a typical low-carbon steel and peritectic steel are presented.<sup>18</sup> Results for a high-carbon steel (0.27%C, not shown) were similar to those of the low-carbon case.

The peritectic steel experiences qualitatively similar behaviour to the ULC steel discussed in the previous section, but its distortion is much more severe. This is because it experiences the well-known extra shrinkage due to the phase transformation from delta-ferrite to austenite. Of equal importance is the high strength of the austenite phase. Thus, peritectic grades experience deeper surface depressions.

In contrast, the low-carbon (0.04%C) steel experiences smaller distortions. This is due to the absence of



5 Temperature and stress profiles through shell during level fluctuation event (5 mm from bottom edge)



6 Effect of level drop distance on shell temperature and distortion (ULC steel)

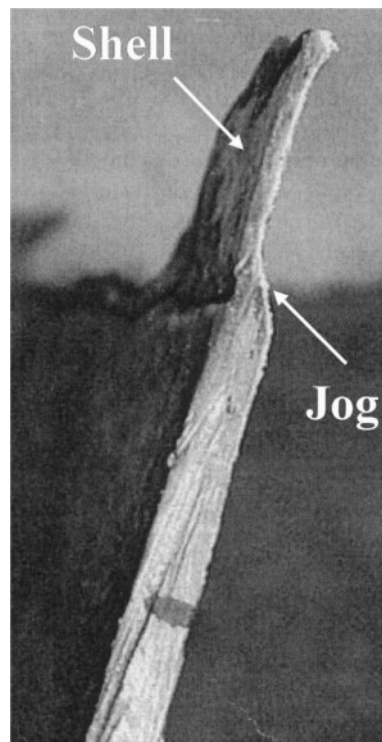
high-strength austenite, combined with the wider mushy zone temperature range (relative to ULC), experienced by this grade. Thus, both the initial shell tip and resolidified skin consist of low-strength delta-ferrite. The high-carbon steel (not shown) has an even wider mushy zone, so it is also very weak. This lack of strength, combined with the lack of phase-transformation shrinkage is responsible for the smooth surface of both the low (eg. 0.04%) and high-carbon (eg. 0.40% C) steels. This matches the changes in surface shape with steel grade that are observed in actual continuous-cast slabs.

### Comparison with measurements

Figure 9 compares the predicted shape of the distorted shell tip in this work with Bikerman's equation for the steady meniscus shape, and with measured hook shapes taken from consecutive oscillation marks on a ULC steel slab cast under conditions in Table 1.<sup>12</sup> The gradual curvature observed in the lower portion of many hooks matches the shape predicted from thermal distortion. This phenomenon also explains the well-known effect of steel grade on oscillation mark depth. Thermal distortion is clearly not responsible for the curved portion of hooks, however, although it might increase their curvature slightly. This result confirms that meniscus solidification is the primary mechanism of curved-hook formation.

Most significantly, level fluctuations deepen the depth of oscillation marks, by increasing thermal distortion. This effect is greatest in peritectic and ULC steels. Furthermore, peritectic steels also experience more severe level fluctuations.<sup>21</sup> This is likely due to sudden variations in the strand thickness below the mould, as the wrinkled surface moves past the surface of the support rolls. Thus, the deeper oscillation marks seen in these grades are caused by several different mechanisms which reinforce each other.

Oscillation mark severity depends on level fluctuations, events during overflow, and steel grade. This work shows how oscillation marks become deeper with increasing depth and duration of level fluctuations. They also become longer and more variable. During overflow, less filling (such as from colder liquid steel), or



7 Jog shape on inside edge of a breakout shell observed by Fredriksson and Elsber<sup>10</sup>

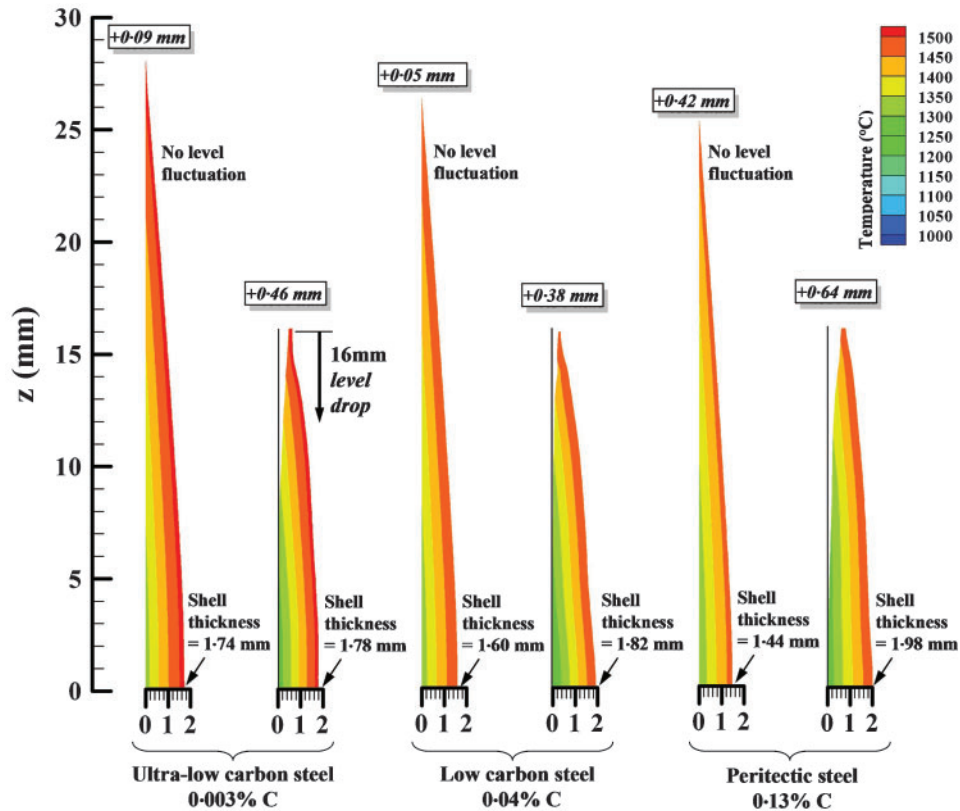
more melting of the interfacial slag layer would also produce deeper oscillation marks.

### Implications for oscillation mark formation mechanism

The computational model results and quantitative metallographic analysis of solidified samples reveal how hooks and oscillation marks form during continuous casting of steel. Thermal distortion is another important factor influencing surface depression and oscillation mark shape during initial solidification. Thermal distortion of the initial shell tip likely controls the shape of the lower portion of oscillation marks, and the formation of shallow, sub-surface straight hooks. It explains the effect of steel grade on oscillation mark depth. As described in detail elsewhere,<sup>1,12,22</sup> curved hooks form by meniscus freezing, followed by overflow that partly fills the gap between the solidified meniscus and the mould wall, and forms the top of the oscillation marks.

### Summary

A finite-element model of thermal-mechanical behaviour of initial solidification has shown that the gradual curved shape of the bottom of oscillation marks depends on thermal distortion. A level fluctuation induces thermal distortion of the shell away from the mould wall. The subsequent rise in liquid level causes the shell to bend even further. Shell distortions of  $\sim 0.5$  mm are predicted for a 0.4 s level fluctuation of 16 mm. Subsequent overflow of the predicted shell shape would create an oscillation mark consistent with observations. Deeper, more-severe level fluctuations produce further bending.



8 Simulated shell distortion for three steel grades with and without level fluctuations: the ULC and peritectic steels exhibit more thermal distortion (compositions given in Table 1)

Peritectic steel grades experience deeper oscillation marks and surface shape variations (wrinkling) due to the extra shrinkage of the  $\delta$ - $\gamma$  phase transformation shrinkage, combined with the high strength of austenite

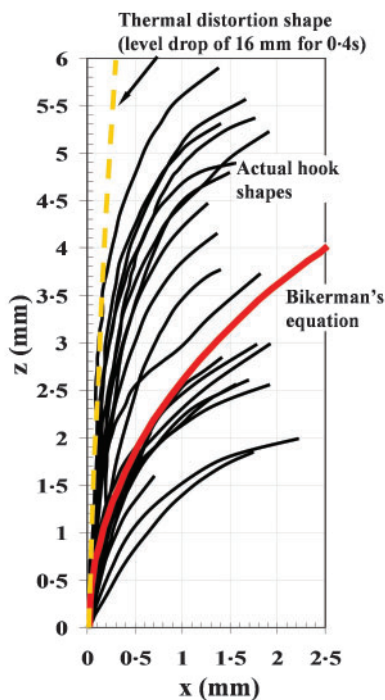
to withstand flattening. In addition, peritectic and ultra-low-carbon (ULC) steels distort much more during level fluctuations, compared with low or high-carbon steels. In ULC steel, this is due to the increase in average shell strength associated with a thin mushy-zone range. The model results predict and explain the observed effect of steel grade on oscillation mark depth and surface depressions.

## Acknowledgements

The authors thank the Continuous Casting Consortium at the University of Illinois, NSERC, the National Science Foundation (Grants), and Labein for funding. Previous work by former graduate students Hong Zhu and Ya Meng (UIUC) for modeling, HoJung Shin and Gogi Lee (Postech), and POSCO Gwangyang Works, Korea for the experimental data is also acknowledged.

## References

1. J. Sengupta, H.-J. Shin, B. G. Thomas, S.-H. Kim: *Acta Materialia* 2006,**54**(4),1165–1173.
2. W. Kurz: Proc. 6th European Conf. on Continuous Casting. Riccione, Italy, June 3–6, 2008., Associazione Italiana di Metallurgia, 2008.
3. E. Takeuchi, J.K. Brimacombe: *Met. Trans B* 1984,**15B**,493–509.
4. R. B. Mahapatra, J. K. Brimacombe, I. V. Samarasekera: *Met. Trans.* 1991,**22B**,875–888.
5. I. V. Samarasekera, J. K. Brimacombe, R. Bommaraju: *ISS Transactions* 1984,**5**,79–105.
6. M. Wolf, W. Kurz: *Metall. Trans. B* 1981,**12B**,85–93.
7. G. Lesoult, J.-M. Jolivet, L. Ladeuille, C.-A. Gandin: In: Solidification Process and Microstructures - A Symposium in Honor of Wilfried Kurz, C.B. M. Rappaz, R. Trivedi, editor., TMS, Warrendale, PA, 2004, 15–26.



9 Line of original of successive hooks on slab samples compared with Bikerman's equation (liquid meniscus shape) and model-predicted shell shape (after level fluctuation)

8. A. Badri, T. T. Natarajan, C. C. Snyder, K. D. Powers, F. J. Mannion, M. Byrne, A. Cramb: *Metallurgical & Materials Transactions B* 2005, **36B**, 373–383.
9. K. Schwerdtfeger, H. Sha: *Metall. Mater. Trans. B* 2000, **31B**, 813–826.
10. H. Fredriksson, J. Elfsberg: *Scandinavian Journal of Metallurgy* 2002, **31**, 292–297.
11. B. G. Thomas, H. Zhu. JIM/TMS Solidification Science and Processing Conference, Honolulu, HI, 1995, 197–208.
12. J. Sengupta, B. G. Thomas, H. J. Shin, G. G. Lee, S. H. Kim: *Metallurgical and Materials Transactions A* 2006, **37A**, 1597–1611.
13. I. G. Saucedo: In: *Mold Operation for Quality and Productivity*. Warrendale, PA, Iron and Steel Society, 1992, 43–53.
14. J. Savage, W. H. Pritchard: *J. Iron Steel Inst.* 1954, **178**, 269–277.
15. G.-G. Lee, Brian G. Thomas, Ho-Jung Shin, Seung-Kwan Baek, Choon-Haeng Choi, Dong-Su Kim, Sung-Jong Yu, S.-H. Kim: *Acta Materialia* 2007, **55**, 6705–6712.
16. C. Li, B. G. Thomas: *Metal. & Material Trans. B.* 2004, **35B**, 1151–1172.
17. P. Kozlowski, B. G. Thomas, J. Azzi, H. Wang: *Metall. Trans. A* 1992, **23A**, 903–918.
18. Y.-M. Won, B. G. Thomas: *Metall. Mater. Trans. A* 2001, **32A**, 1755–1767.
19. H. Zhu: Ph.D Thesis, University of Illinois, 1993.
20. J. Parkman: Mechanical and Industrial Engineering; Urbana, IL: University of Illinois at Urbana-Champaign, 2000.
21. G. Xia, C. Bernhard, S. Ilie, C. Fuerst: Proc. 6th European Conf. on Continuous Casting. Riccione, Italy, June 3–6, 2008., Associazione Italiana di Metallurgia, 2008.
22. G.-G. Lee, Ho-Jung Shin, Brian G. Thomas, Seon-Hyo Kim, S.-J. Yu: Proc. Int. Conf. Steelmaking, AISTech 2007, vol. 1. Indianapolis, IN, May 7–10, 2007, AISTech, Warrendale, PA, 2007.